

Metallicity in the Galactic Center: The Quintuplet cluster

Francisco Najarro¹, Don F. Figer², D. John Hillier³, T. R. Geballe⁴, Rolf P. Kudritzki⁵

najarro@damir.iem.csic.es

ABSTRACT

We present a measurement of metallicity in the Galactic center Quintuplet Cluster made using quantitative spectral analysis of two Luminous Blue Variables (LBVs). The analysis employs line-blanketed NLTE wind/atmosphere models fit to high-resolution near-infrared spectra containing lines of H, He I, Si II, Mg II, and Fe II. We are able to break the H/He ratio vs. mass-loss rate degeneracy found in other LBVs and to obtain robust estimates of the He content of both objects. Our results indicate solar iron abundance and roughly twice solar abundance in the α -elements. These results are discussed within the framework of recent measurements of oxygen and carbon composition in the nearby Arches Cluster and iron abundances in red giants and supergiants within the central 30 pc of the Galaxy. The relatively large enrichment of α -elements with respect to iron is consistent with a history of more nucleosynthesis in high mass stars than the Galactic disk.

Subject headings: Galaxy: abundances – stars: abundances – stars: individual (Pistor Star, FMM362) – infrared: stars – Galaxy: center

1. Introduction

Elements heavier than hydrogen and helium (“metals”) are primarily created by nucleosynthesis in stars. Metals are important ingredients in many astrophysical processes such

¹Instituto de Estructura de la Materia, CSIC, Serrano 121, 29006 Madrid, Spain

²Chester F. Carlson Center for Imaging Science, Rochester Institute of Technology, 54 Lomb Memorial Drive, Rochester, NY 14623

³Department of Physics and Astronomy, University of Pittsburgh, 3941 O’Hara Street, Pittsburgh, PA 15260

⁴Gemini Observatory, Hilo, 670 N. A’ohoku Pl., HI 96720

⁵Institute for Astronomy, University of Hawaii, 2680 Woodlawn Drive, Honolulu, HI 96822

as radiative cooling, and mass-loss during star formation and at all stages of stellar evolution. They also play a fundamental role in stellar evolution through their influence on stellar opacities, and represent a historical record of galactic chemical enrichment via stellar winds and supernovae ejecta.

In the Galaxy metal abundance increases with decreasing galactocentric radius, as seen in stars and gas (Afflerbach et al. 1997; Rudolph et al. 2006; Maciel & Quireza 1999; Fuhrmann 1998; Rolleston et. al. 2000; Smartt et. al. 2001; Luck et al. 2006). Other galaxies show a similar trend, having highest metal abundances in their nuclei (Urbaneja et al. 2005; Kennicutt et. al. 2003).

Previous work (Frogel et al. 1999; Feltzing & Gilmore 2000; Carr et al. 2000; Ramirez et al. 1997, 1999, 2000) on the Galactic center (GC) has indicated roughly solar stellar metal abundances, whereas the analyses of interstellar emission lines (Shields & Ferland 1994; Maeda et al. 2000) have suggested considerably higher abundances. It is not clear why the stellar and gas-phase measurements should differ so greatly.

The GC contains three dense and massive star clusters that have recently formed in the inner 50 pc, the Arches, Quintuplet, and Central clusters. Using quantitative spectral analysis, Najarro et al. (2004) (Paper I) determined that the WNL stars in the very young (2-2.5 Myr) Arches Cluster have roughly solar metallicities. Being more evolved (~ 4 Myr), the Quintuplet Cluster (Glass et al. 1987, 1990; Nagata et al. 1990; Okuda et al. 1990; Moneti et al. 1994) contains a variety of massive stars, including WN, WC, WN9/Ofpe, luminous blue variables (LBVs) and less evolved blue-supergiants (Figer, McLean, & Morris 1995; Figer et al. 1999a,b). Two LBVs in it are known, the Pistol Star (Moneti et al. 1994; Cotera et al. 1994; Figer, McLean, & Morris 1995; Figer et al. 1998, 1999c) and FMM362 (Figer et al. 1999b; Geballe, Najarro, & Figer 2000), each having an infrared spectrum rich in metal lines of Fe II, Si II, & Mg II.

In this paper, we use quantitative infrared spectroscopy of the two Quintuplet LBVs to make direct determinations of metallicity in those stars. We also use the derived α -elements vs. Fe ratio to address the dominance of massive stars on the IMF in this region.

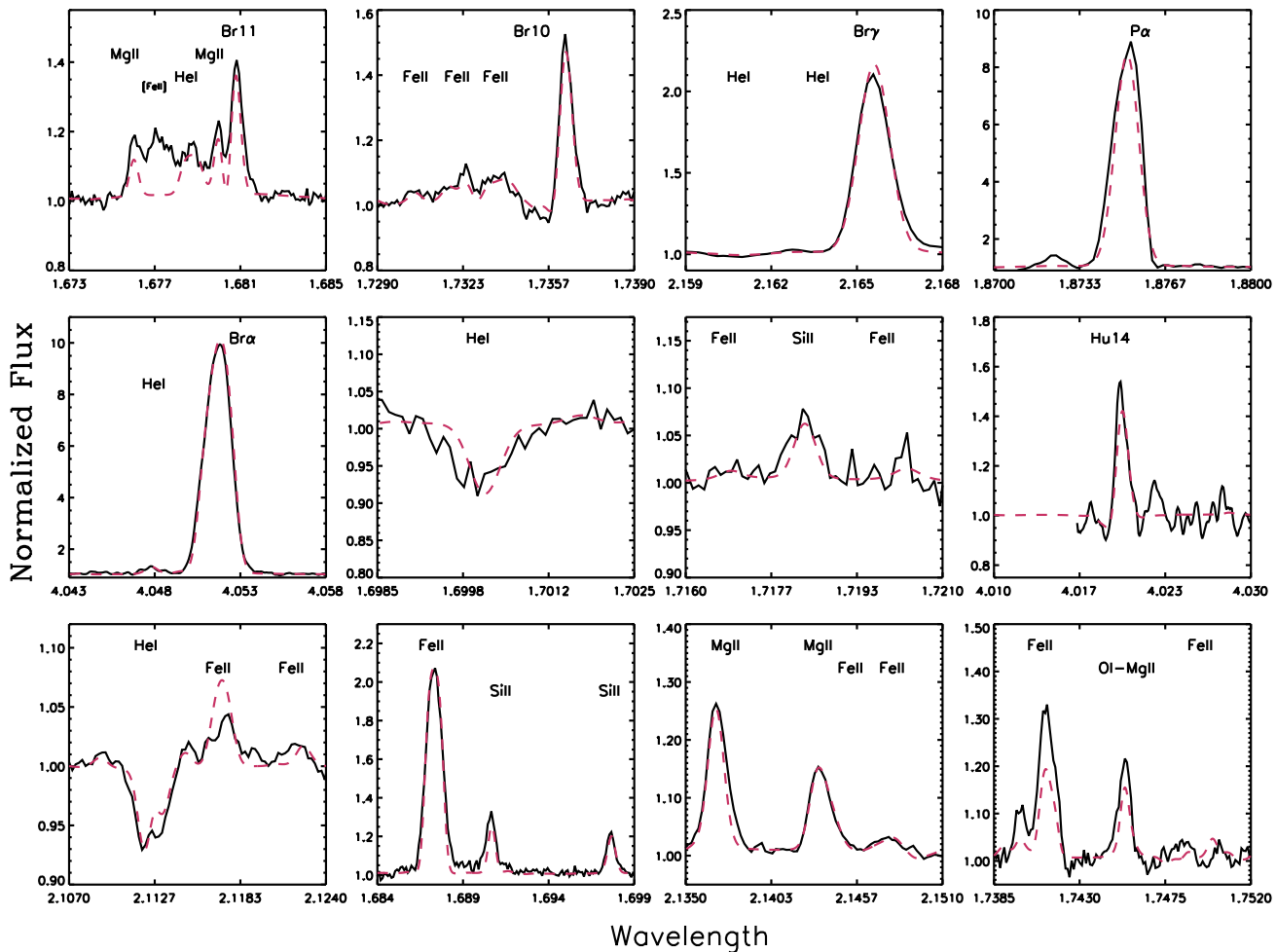


Fig. 1.— Model fits (*dashed lines*) to the observed infrared diagnostic lines (*solid lines*) of the Pistol Star. The forbidden [Fe II] line at $1.677 \mu\text{m}$ was not included in the models.

2. Observational Data

The data were obtained at UKIRT¹ using CGS4. The Pistol Star was observed in April 1996 (P α ; R \sim 3000), July 1997 (L; R \sim 16000) and April 1998 (H; R \sim 5000 and K R \sim 3000). Likewise, spectra for FMM362 were obtained in April (L) and May 1999 (H and K), using CGS4 in medium resolution mode (R \sim 5,000-6,500). The slit width was 0'6 for all observations. We used the photometric measurements of Figer et al. (1998) for the Pistol Star, to scale the reduced spectra. For FMM362, given its photometric variability, we adopted the average value, K=7.30, obtained by Glass et al. (1999) for the epoch closest to our spectroscopic observations. This value agrees, within the 0.26 standard deviation derived by Glass et al. (1999), with the K=7.50 value adopted by Geballe, Najarro, & Figer (2000) from flux-calibrated spectra. We assume the same extinction for both objects and adopt the value of $A_K=3.2$ derived by Figer et al. (1998) for the Pistol Star. The reader is referred to these papers for a detailed discussion on the reduction of the observed spectra and photometry.

3. Models

To model the LBVs and estimate their physical parameters, we have used CMFGEN, the iterative, non-LTE line blanketing method presented by Hillier & Miller (1998) which solves the radiative transfer equation in the co-moving frame and in spherical geometry for the expanding atmospheres of early-type stars. The model is prescribed by the stellar radius, R_* , the stellar luminosity, L_* , the mass-loss rate, \dot{M} , the velocity field, $v(r)$ (defined by V_∞ and β), the volume filling factor characterizing the clumping of the stellar wind, $f(r)$ (see Sec. 4.2), and elemental abundances. Hillier & Miller (1998, 1999) present a detailed discussion of the code. For the present analysis, we have assumed the atmosphere to be composed of H, He, C, N, O, Mg, Si, S, Fe and Ni. Given the parameter domain the LBVs are located, the $\tau = 2/3$ radius is located close or above the sound speed, and therefore the assumed hydrostatic structure plays no role. Thus, no spectroscopic information about the mass of the object can be obtained. The atomic data sources are described in detail Hillier et al. (2001). Here we focus on the model atoms used for our abundance determinations Fe II, Mg II and Si II. Using the superlevel formalism (NS/NF, number of superlevels vs. number of levels in the full atom, e.g. Hillier & Miller 1998) we chose 233/709 (up to 109800 cm^{-1}) for Fe II, 37/50 (up to 119400 cm^{-1}) for Mg II and 35/72 (up to 125000 cm^{-1}) for Si II. The choice

¹The United Kingdom Infrared Telescope (UKIRT) is operated by the Joint Astronomy Centre on behalf of the Particle Physics and Astronomy

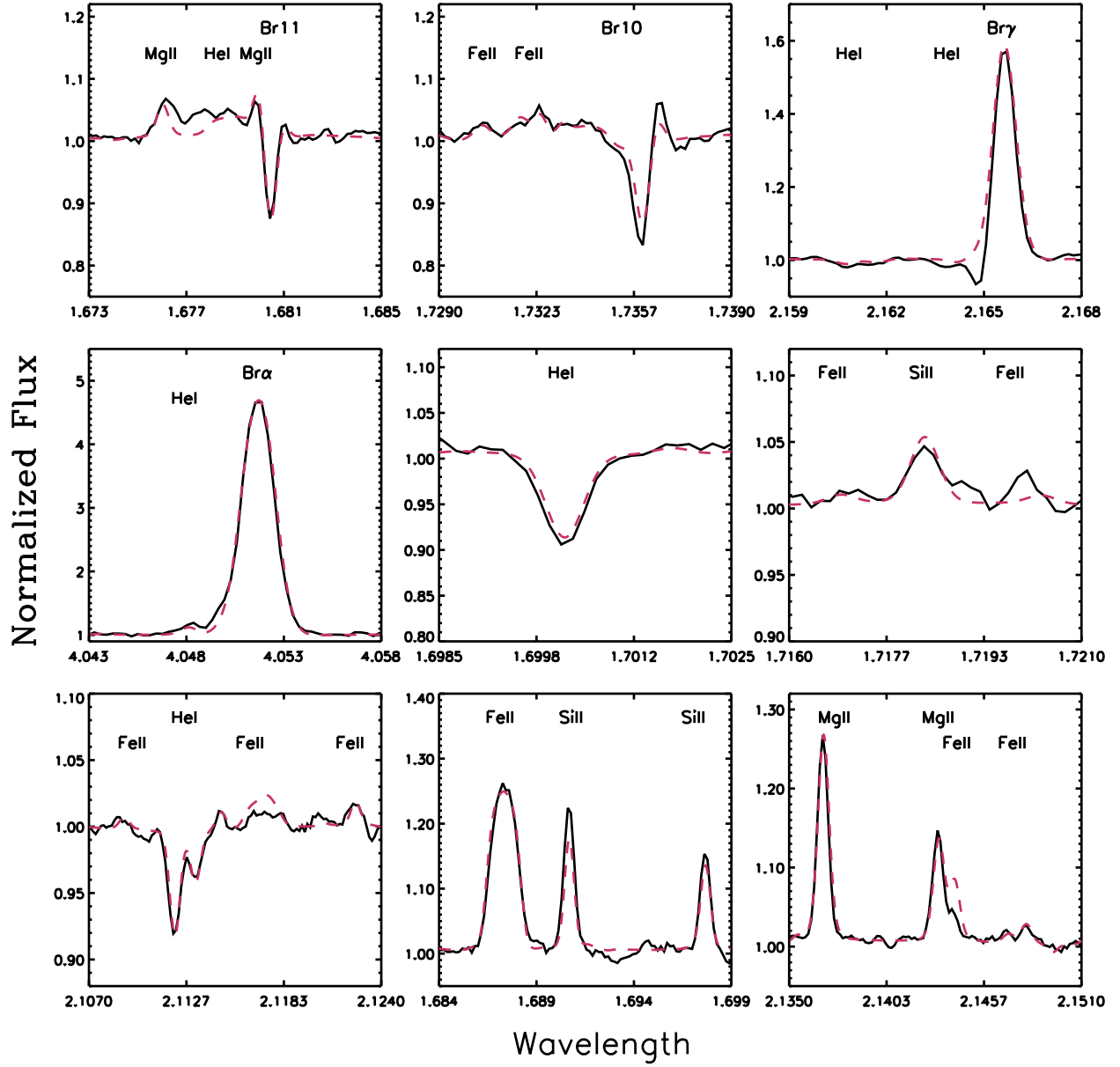


Fig. 2.— Model fits (*dashed lines*) to the observed infrared diagnostic lines (*solid lines*) of FMM362.

of the appropriate packing has been extensively tested in Najarro (2001). We will revise the importance of this issue for the case of Mg in 4.4.

Observational constraints are provided by the H, K and L-band spectra of the stars and the dereddened K magnitudes from Figer et al. (1998), Geballe, Najarro, & Figer (2000) and Glass et al. (1999). As in Paper I, a distance of 8 kpc has been assumed. The validity of our technique has been demonstrated in Najarro et al. (1999) and Najarro (2001) by calibrating our method against stars with similar spectral type such as P Cygni and HDE 316285 for which not only infrared but also optical and UV spectra are available.

4. Results

Table 1 gives the derived stellar parameters for both LBVs and Figs. 1 and 2 show model fits to the relevant lines in the stars. Theoretical spectra have been convolved with the instrumental resolution. We note that given the large number of parameters involved in the analysis it is unaffordable to perform a full systematic error analysis in the whole parameter domain. We rather proceed by estimating the range of values for the main stellar parameters which provide acceptable fits to the observed spectra. Once those ranges are set, we derive the corresponding abundances and their errors. From Table 1, it can be seen that the Pistol Star and FMM362 have very similar properties, with the exceptions of the Pistol Star’s significantly higher wind density (evidenced by the its stronger spectral lines) and its higher He content. The latter may denote a slightly advanced evolutionary stage for the Pistol Star (see below). Given the general resemblance of the spectra of the objects, we discuss them together.

4.1. Main Diagnostic Lines and Stellar Properties

Several spectral diagnostics constrain our estimates of the stellar temperature, and thus the ionization structure, in particular the He I (5-4) components near $4.05 \mu\text{m}$. If helium is predominantly singly ionized, even for the most favorable case with (minimum) cosmic helium abundance, the observed ratio of H to He I lines exceeds the expected values by large factors. This indicates that He II must recombine to He I very close to the photosphere, implying an upper limit of around 13,000 K for the temperatures of these objects. We find a lower limit of 10,000 K for the temperatures, as lower values would require non-detection of the He I components. Also the strengths of the He I $1.700 \mu\text{m}$ and He I $2.112/3 \mu\text{m}$ lines are very sensitive to temperature, so that they appear in emission above 12,500 K and vanish below

Table 1. Derived stellar parameters

Parameter	Pistol	FMM362
$L_*(10^6 L_\odot)$	1.60	1.77
$R_{2/3} (R_\odot)$	306	350
$T_{\text{eff}}(10^4\text{K})$	1.18	1.13
H/He	1.5	2.8
Fe/Fe $_\odot$	1.1 (0.78)	1.1 (0.78)
Mg/Mg $_\odot$	2.2	1.5
Si/Si $_\odot$	1.8	2.1
$\dot{M}(10^{-5} M_\odot \text{ yr}^{-1})$	2.1	1.2
β	3.0	1.3
$V_\infty(\text{km s}^{-1})$	105	170
$D_{\text{mom}}=\log(\dot{M}V_\infty(R/R_\odot)^{1/2})$	29.39	29.38
$M_{\text{Edd}} (M_\odot)$	22.5	30.5
CL $_1$	0.08	0.08
CL $_2$	2.5	2.00
CL $_3$	2.00	–

Note. — β is the exponent describing the velocity field, D_{mom} is the modified wind momentum (Kudritzki & Puls 2000) and clumping parameter, the CL are defined in Eq. 1. M_{Edd} are the Eddington masses. H/He is the ratio by number, and other abundances are relative to solar after Grevesse & Noels (1993). The Fe abundance relative the value in Anders & Grevesse (1989) is given in parentheses (see text).

10,500 K. These lower limits on the effective temperature are also consistent with the non-detections of the Si II $3s^23p^2S_{1/2}-3s^24p^2P_{3/2}$ 2.180 μm and $3s^23p^2S_{1/2}-3s^24p^2P_{1/2}$ 2.209 μm intercombination lines, as they are expected to appear strongly in absorption as soon as the temperature drops below 10,000 K. Hence, $\Delta T \pm 1500$ K are conservative estimates of uncertainties for the temperatures of the Pistol Star and FMM362 given in Table 1.

To estimate the terminal velocities, we make use of the Fe II] (semi-forbidden Fe II) $z^4F_{9/2}-c^4F_{9/2}$ 1.688 μm line (Geballe, Najjarro, & Figer 2000; Figer et al. 1998) that forms in the outer wind and has a weak oscillator strength ($gf \sim 10^{-5}$). This is because non-negligible continuum opacity effects at 4 μm may provide only lower limits if Br α is used. The larger V_∞ derived for FMM362 can be clearly inferred from the width of this Fe II] line and the obvious overlap at Br α between the H I and He I components (see Fig. 2). For the Pistol Star (Fig. 1) the Br α components are fairly well separated.

Our analysis of wind density (\dot{M} , β) gives values of β that agree with those inferred in the literature for other LBVs (Najarro 2001) and B-Supergiants (e.g Crowther et al. 2006). The values are fairly well constrained by the shapes of the hydrogen lines, especially those of Br α and Br γ which are inconsistent with the same value of β for both objects.

Although the wind density derived for the Pistol Star is much higher than for FMM362, the modified wind momenta $D_{mom} = \log(\dot{M}V_\infty\sqrt{R/R_\odot})$ (Kudritzki & Puls 2000) of the two LBVs are nearly identical (Table 1). This result is qualitatively consistent with the wind momentum - luminosity relation (Kudritzki & Puls 2000) which predicts the same modified momenta for objects with the same stellar type and luminosity. Note that we have used clumping-corrected values of \dot{M} to compute the modified momenta. If unclumped values were assumed, D_{mom} would be closer to 30.0. Interestingly, the latter agrees very well with the averaged modified momentum of AG Car at maximum (i.e., at similar T_{eff} to our objects) obtained using the values of \dot{M} , V_∞ and R_* derived by Stahl et al. (2001) from fits to H α . Those authors obtained $\log(\dot{M}) \sim -4.1$ for about this temperature, while our unclumped values are $\log(\dot{M}) = -4.1$ and -4.4 for the Pistol Star and FMM362 respectively. Further, using radiation-driven wind models for LBVs, Vink & de Koter (2002) were able to predict the Stahl et al. (2001) \dot{M} value for AG Car assuming $V_\infty/V_{\text{esc}} \sim 1.3$ and a current stellar mass of $35M_\odot$. The same value of V_∞/V_{esc} for the LBVs would imply current stellar masses of $27.5M_\odot$ for the Pistol Star and $46M_\odot$ for FMM362. Although these masses should be regarded with caution, they are consistent with the Pistol Star being more evolved than FMM362 (as inferred from their He/H ratios) and hence having lost more mass during its evolution, as indicated by the presence of a nebula around it.

Compared to the results obtained in Figer et al. (1998) by means of non-blanketed models, the new blanketed models provide a significant improvement in our knowledge of

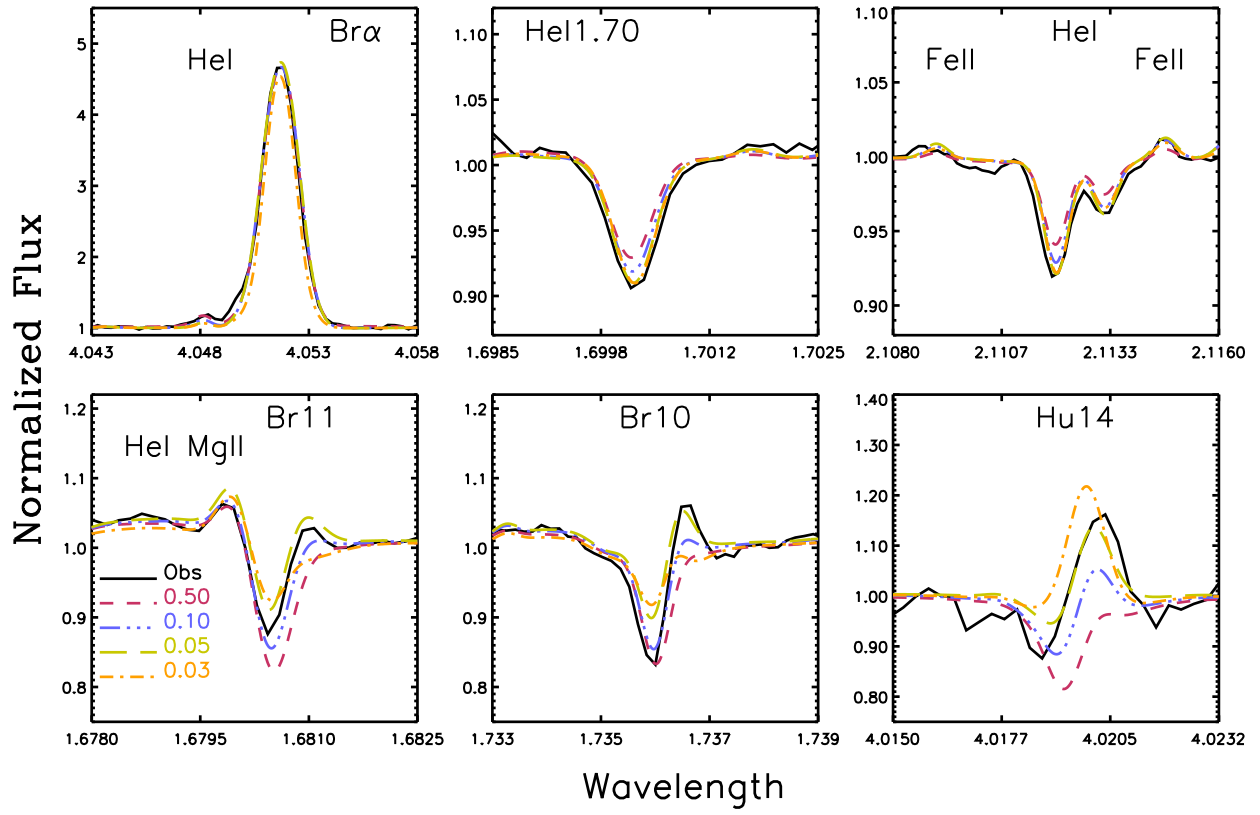


Fig. 3.— Model spectra showing the effect of clumping parameter CL_1 (see Eq.1) on diagnostic line profiles of FMM362. Values of CL_1 are listed in the bottom left panel.

the physical properties of these two stars. The degeneracy of the “high” and “low” luminosity (T_{eff}) solutions for the Pistol Star presented by Figer et al. (1998) is broken by the Si II, Mg II and Fe II lines, which are clearly more consistent with the “low” solution. We derived for this star a luminosity of $\sim 1.6(10^6) L_{\odot}$, an effective temperature of $\sim 11,800$ K, and an initial mass of $100 M_{\odot}$. The stellar luminosity is reduced by a factor of two compared with the previous estimate, illustrating the importance of the new generation of line-blanketed models. Below, we discuss in detail the role of two additional stellar properties that are derived using the new models, wind clumping and elemental abundances.

4.2. Clumping

Clumping is normally invoked in stellar winds to explain inconsistencies arising between ρ (density) and ρ^2 diagnostics. For a given mass-loss, clumping causes an enhancement of ρ^2 processes while leaving unaltered those which depend linearly on ρ . Further, if mass-loss rate and clumping are scaled without changing the $\dot{M}/f^{0.5}$ ratio, the ρ -dependent diagnostics vary while the recombination lines profiles ($\propto \rho^2$) remain basically unaltered.

To investigate the clumping we introduce the following clumping law:

$$f = CL_1 + (1 - CL_1)e^{\frac{-V}{CL_2}} + (CL_4 - CL_1)e^{\frac{(V-V_{\infty})}{CL_3}} \quad (1)$$

where CL_1 and CL_4 are volume filling factors and CL_2 and CL_3 are velocity terms defining locations in the stellar wind where the clumping structure changes. CL_1 sets the maximum degree of clumping reached in the stellar wind (provided $CL_4 > CL_1$) while CL_2 determines the velocity of the onset of clumping. CL_3 and CL_4 control the clumping structure in the outer wind. Hence, when the wind velocity approaches V_{∞} , so that $(V - V_{\infty}) \leq CL_3$, clumping starts to migrate from CL_1 towards CL_4 . If CL_4 is set to unity, the wind will be unclumped in the outermost region. Such behavior was already suggested by Nugis et al. (1998) and was utilized by Figer et al. (2002) and Najarro et al. (2004) for the analysis of the WNL stars in the Arches Cluster. Recently, Puls et al. (2006) also have found similar behavior from H α and radio studies of OB stars with dense winds. Furthermore, our clumping parametrization is consistent with results from hydrodynamical calculations by Runacres & Owocki (2002). From Eq. 1 we note that if CL_3 , and therefore CL_4 , is not considered ($CL_3 \rightarrow 0$), we recover the simpler variation proposed by Hillier & Miller (1999). To avoid entering free parameters heaven we set $CL_4 = 1$ in all of our investigations, aiming to get an appropriate amount of leverage on the amount of non-constant clumping in the outer wind regions.

CL₁: Estimating the wind clumpiness. Figure 3 illustrates the sensitivity to CL_1

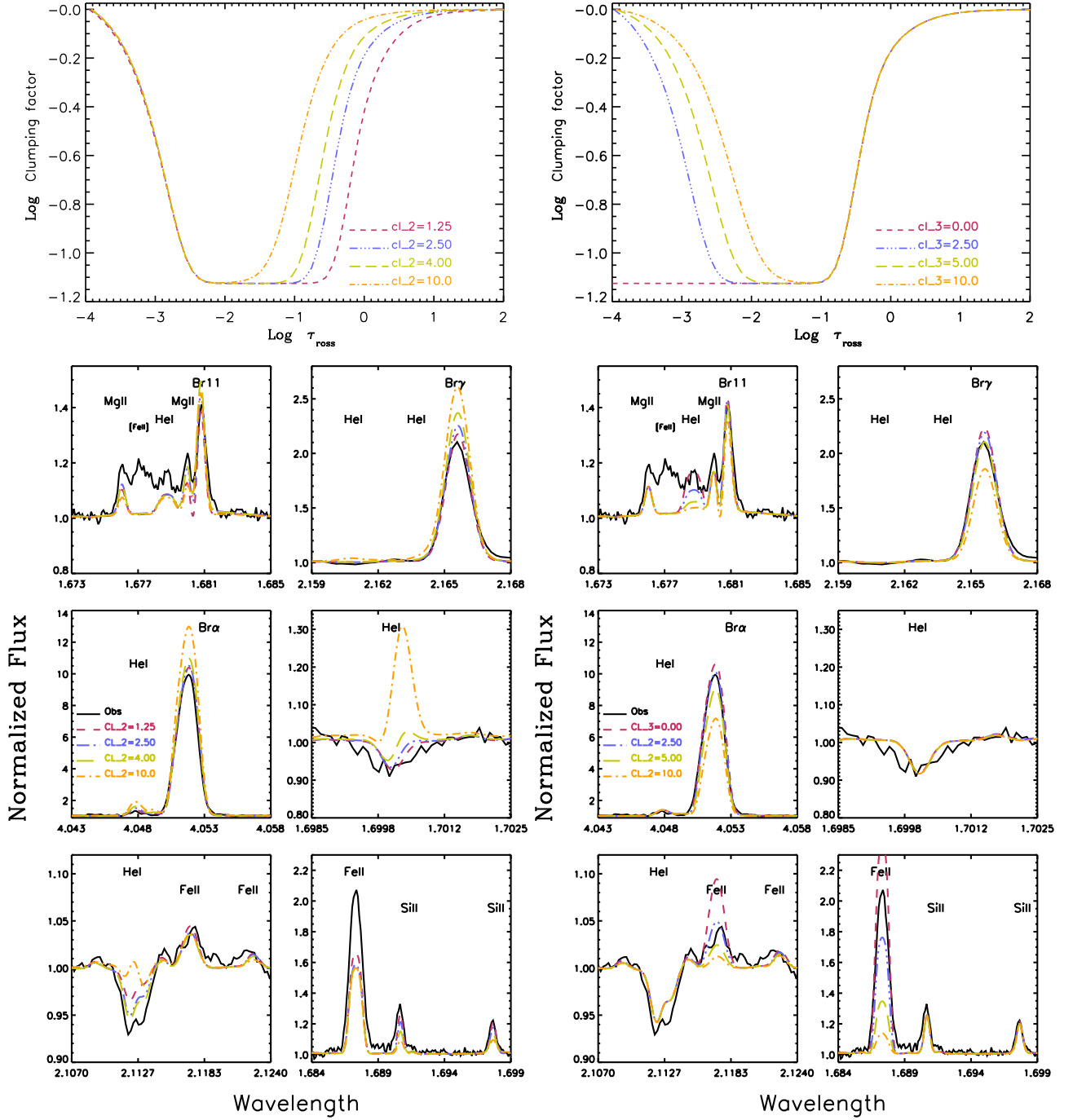


Fig. 4.— Influence of adopted clumping structure (see Eq. 1) in profiles. Run of clumping and line profile sensitivities for different values of CL_2 (left panel) and CL_3 (right panel), compared to observed profiles in the Pistol Star. See discussion in text.

of the main diagnostic lines utilized to obtain the degree of clumping in the stellar winds of FMM362. For each value of CL_1 displayed in Fig. 3 the mass-loss rate in the model was scaled while keeping $\dot{M}/f^{0.5}$ constant as described previously. Although there are some lines that follow this scaling quite well ($B\alpha$, and also $B\gamma$ and some metal lines not displayed in the figure), the He I lines and weak H I lines react quite sensitively to the absolute degree of wind clumping. It can be seen that the He I lines only provide an upper limit to CL_1 (a bit lower than 0.1) and do not react to lower values, but a unique value for CL_1 can be selected by some H I lines. The Hu_{14} (H I(14-6)) line displays the highest sensitivity to clumping. Unfortunately, the wavelength interval surrounding this line was not observed with sufficiently high S/N in FMM362 and there is a large uncertainty in the continuum value, which is critical for estimating CL_1 . We could make full use of the Hu_{14} line to determine the clumping only for the Pistol Star, where this line is relatively stronger in emission (see Fig. 1). Nevertheless, Fig. 3 shows that CL_1 lies between 0.1 and 0.05. It must be stressed that only with a well determined clumping may we address the He/H abundance issue (see Sec. 4.3).

CL_2 & CL_3 : Mapping the clumping structure. The upper panels of Fig. 4 illustrate the behavior of the clumping structure for different sets of CL_2 and CL_3 values, while the lower panels display the influence of such behavior on diagnostic lines in the spectrum of the Pistol Star. It is evident that for some spectral lines e.g., He I 2.112 μm , the behavior of the profiles with clumping is far from being monotonic. Furthermore, not only do lines of different ions react differently to clumping, but also lines within the same ion, e.g., H I, behave differently. For example, Fe II does not respond in the same way to changes in CL_2 and CL_3 . Figure 4 shows the great potential of the different IR lines to constrain the clumped structure of the stellar wind and demands the following detailed discussion.

The general impact of clumping on line profiles that was described at the beginning of this section will occur provided the ionization equilibrium is on the “safe” side. We consider the “safe” region to be where the population of the next ionization stage clearly dominates over the one the line belongs to (i.e., $H\text{II} \gg H\text{I}$ for the hydrogen lines). Noting, however, that ionization depends linearly on density whereas recombination is proportional to ρ^2 , a “changing” ionization situation may occur, where two adjacent ionization stages have similar populations. In such a case clumping, which enhances recombination, will cause a net reduction of the mean ionization. This will result in weaker lines.

Finally, in the infrared, via bound-free and free-free processes ($\propto \rho^2$), not only the lines but also the continuum will depend on clumping, resulting in high sensitivity of the continuum-rectified line profiles to CL_1 and CL_2 .

One may, therefore, distinguish between lines formed on the “safe” region and those

arising from the “changing” region. Within the parameter domain of the two LBVs studied here we find that H I, Si II, and Mg II lines and also the Fe II photospheric lines are formed in “safe” regions, while He I and Fe II] lines arise from “changing” regions.

Increasing the clumping (decreasing the CL_1 value), or alternatively decreasing the velocity at which clumping sets in (decreasing CL_2) results in stronger Si II and Mg II lines, as shown in Fig. 4-left. The strong H I lines are formed further out than the Si II and Mg II lines and their strengths should in principle show no sensitivity to CL_2 . However, the continuum is clearly affected by clumping. Thus the stronger the clumping (lower CL_2), the stronger the continuum and the weaker the resulting line-to-continuum ratio, as clearly shown by $B\gamma$ and $B\alpha$ in Fig. 4-left. On the other hand, weaker H I lines such as H_{14} or B_{10} and B_{11} form much closer to the photosphere and tend to brighten with increasing clumping. The weak Fe II lines formed close to the photosphere react in basically the same way as the continuum and thus the normalized spectra of them show no changes with changing clumping. Their near independency allows these lines to be used as Fe abundance indicators (see below). The Fe II] lines, formed even beyond the H I lines, are affected by two competing processes. On one hand, increasing the extent of the clumped region (decreasing CL_2) results in a reduction of the Fe III/Fe II ratio in the wind. Since Fe III remains the dominant ionization stage in the Fe II] line formation zone, this change will cause a slight increase in the strengths of the Fe II] lines. On the other hand, as the continuum increases with increasing clumping, the line-to-continuum ratio decreases. Thus the two processes counter-balance (see Fig. 4-left). Finally, the He I lines, which form close to the photosphere, show weak continuum dependences, but high sensitivities to ionization/recombination. Thus, starting with the model with the highest CL_2 values, the He I lines are not affected by clumping, but the stellar parameters produce strong ionization in the inner parts resulting in overly strong emission (He I $1.700 \mu\text{m}$) and line filling (He I $2.112 \mu\text{m}$). However, as clumping is enhanced in the line formation zone, recombination starts to dominate over ionization and the He I line emission weakens, the lines are no longer as filled, and start to appear in absorption.

Regarding clumping in the outer parts of the wind, it can be seen on the right side of Fig. 4 that only the strong H I and Fe II] lines react to CL_3 . Note that $B\alpha$ which forms further out than $B\gamma$ is more sensitive to clumping and the observed ratio of the two profiles may be used to determine CL_3 . For winds of significantly lower density, these lines will form further in and show little or no dependence on CL_3 (e.g., FMM362). The Fe II] lines are more sensitive to CL_3 , primarily due to the coupling of the Fe ionization structure with that of hydrogen thru charge-exchange reactions in the outer wind zones where H II starts to recombine. Due to the difference in H and Fe abundances, a small and hardly noticeable change in the ionization of hydrogen will be amplified in the Fe III/Fe II ratio, resulting in a large change in iron recombination. Thus, decreasing CL_3 dramatically enhances the Fe II]

lines, as shown in on the right side of Fig. 4. The H I lines behave similarly to the way they do in “safe” regions.

For the Pistol Star the best fits to the various line profiles suggest a decreasing clumping factor that becomes unity in the outer wind, whereas for the less dense wind of FMM362, the line profiles are best matched by a constant clumping factor. From the clumping estimates, we find uncertainties of 0.10 dex in the mass-loss rates. The value of $CL_1 = 0.08$ obtained for each star is somewhat low compared to the values derived for other LBVs such P Cygni ($CL_1=0.5$, Najarro 2001) or AG Car ($CL_1=0.25$, Groh et al. 2006) and is more consistent with those derived for WR stars ($CL_1\sim 0.1$, Herald et al. 2001; Najarro et al. 2004). We note, however, that the LBVs have higher He abundances than P Cygni, pointing to a more evolved status, closer to the WR phase.

4.3. H/He ratio. Breaking the degeneracy

Hillier et al. (1998) showed that for HDE 316285, an LBV-like star with similar T_{eff} and slightly higher wind density than the Pistol Star, a degeneracy exists between the H/He ratio and the mass-loss rate. In principle, fits of virtually equal quality could be obtained with H/He ratios varying from 0.05 to 10 by scaling the mass-loss rate. Such a degeneracy, if present in the Quintuplet LBVs, would imply that if the H/He ratio falls below a certain value ($H/He\leq 2$), the resulting metal abundances could be scaled down to obtain the same line strengths. Hence one could obtain only an upper limit on the metal abundances. breaking this degeneracy is crucial to understanding the evolutionary status of these objects.

Because of the lower wind density of the Quintuplet LBVs and the sensitivities of some of the infrared lines to the stellar parameters, we are able to break the H/He degeneracy and obtain robust estimates of their He content. Due to the high degree of clumping found in both objects, the $\tau = 2/3$ radius, where T_{eff} is defined, is reached at considerably lower velocities than for classical LBVs. Thus, wind speeds roughly between half and one-third of the sound speed are found in the Pistol Star and FMM362 while classical LBVs have wind speeds well above the speed of sound (Hillier et al. 1998; Najarro 2001). This enables quasi-photospheric absorption lines to form. The He I 2.112 μm line is the key in breaking the degeneracy. This is shown for FMM362 in Fig. 5, which contains model spectra computed for H/He ratios ranging from H/He=5.0 to 0.75, with mass-loss rates and metal abundances scaled and the other stellar parameters fine-tuned to reproduce the observed profiles of other lines. The figure shows that while identical H I and He I (He I 1.700 μm) line profiles (also for the rest of hydrogen and metal lines) are obtained for all H/He ratios considered, the absorption *depths* of the He I 2.112 μm and He I 2.15 μm lines react sensitively to the He

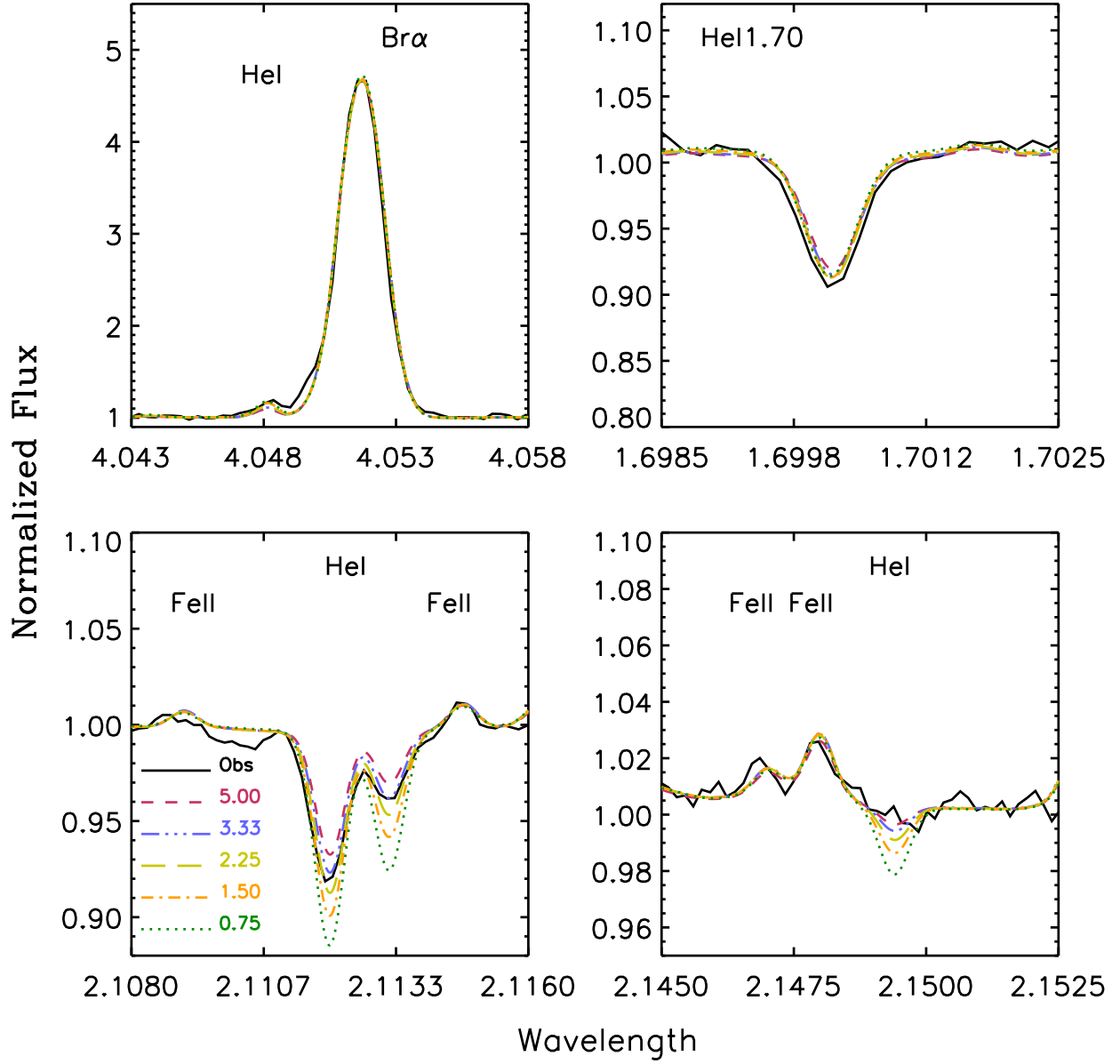


Fig. 5.— Breakdown of the H/He degeneracy in FMM362. Models with H/He ratios ranging from 5.0 to 0.75 provide identical H I and strong He I line profiles, but weaker He I profiles can be used to determine the He abundance (see text)

abundance. Both lines show that the best H/He value must lie between 3.33 and 2.25, and we find a most likely value of 2.8 (see Table 1). Similar behavior was found for the Pistol Star, where we obtain H/He=1.5.

4.4. Metal Abundances

For the purpose of discussing metal abundances (see Table 2), we adopt the solar composition of Grevesse & Noels (1993). Although their abundances have been recently revised (Asplund et al. 2005; Allende Prieto 2008) (but see also Pinsonneault & Delahaye (2006)), they are the ones used by Iglesias & Rogers (1996) to compute stellar interior opacities and adopted in the most recent evolutionary models for massive stars with rotation from the Geneva group (Meynet & Maeder 2003, 2005), and the Padova tracks used for cooler, less massive stars (Girardi et al. 2000; Salasnich et al. 2000). Previously published evolutionary tracks for massive stars (Schaller et al. 1992; Meynet et al. 1994) used opacity tables calculated with solar composition from Anders & Grevesse (1989), which differ significantly from Grevesse & Noels (1993) only in Fe ($A(\text{Fe}/\text{H})=7.67$ vs 7.50 in Grevesse & Noels (1993))² and very slightly in the CNO ratios ($A(\text{C}/\text{H})=8.56$, $A(\text{N}/\text{H})=8.05$, $A(\text{O}/\text{H})=8.93$ in Anders & Grevesse (1989) vs $A(\text{C}/\text{H})=8.55$, $A(\text{N}/\text{H})=7.97$, $A(\text{O}/\text{H})=8.87$ in Grevesse & Noels (1993)). Nevertheless, we have also listed in Table 1, in parentheses, the measured abundances with respect to the solar Fe values from Anders & Grevesse (1989). Si and Mg are the same in all evolutionary models, and have been only slightly revised downward (~ 0.05 dex) by Asplund et al. (2005). Thus, the reader should note that current discussions found in the literature on the derived α -elements vs. Fe ratio may depend critically on the assumed Fe solar abundance.

Iron. Two types of Fe II lines are found in the spectra³. The first are the strong semi-forbidden lines, including $z^4F_{9/2}-c^4F_{9/2}$ $1.688 \mu\text{m}$ and $z^4F_{3/2}-c^4F_{3/2}$ $2.089 \mu\text{m}$, that form in the outer wind and have small oscillator strengths ($gf \sim 10^{-5}$). The second are the weak permitted ($gf \sim 1$) lines connecting higher lying levels, such as the $4d^6G-5p^6F$ lines near $1.733 \mu\text{m}$ or $6p^6D-6s^6D$ at $2.109 \mu\text{m}$, that form much closer to the photosphere.

The permitted lines are more robust iron abundance indicators, having only weak dependences on other parameters, such as turbulent velocity. The strengths of the semi-forbidden lines depend on the accuracy of their weak gf values, the mass loss rate and the run of the

² $A(X/Y)=\log[n(X)/n(Y)]+12$

³The forbidden [Fe II] $1.677 \mu\text{m}$ line present in the Pistol Star is not included in our models

iron ionization structure in the outer wind, which is sensitive to the hydrogen ionization structure due to the strong coupling to the Fe/H charge-exchange reactions. Since a change in the run of the clumping factor in the outer wind regions modifies the ratio of recombinations/ionizations in hydrogen, the semi-forbidden lines are diagnostic of the behavior of clumping there. From Fig. 1 it can be seen that that our model is able to simultaneously reproduce both sets of lines, providing constraints on both clumping and abundance.⁴

We obtain roughly solar iron abundances for both LBVs, with ± 0.15 dex as plausible uncertainties (see Fig. 7). Our results are similar to $A(\text{Fe}/\text{H})=7.59$ recently derived by Cunha et al. (2007) from their analysis of a sample of luminous cool stars within 30 pc of the Galactic Center. Note in Table 1 that the Fe abundance ratio has significant uncertainty due to the uncertainty in the Fe abundance in the Sun.

Magnesium. The strongest Mg II lines observed in the H and K bands share the $5p^2P$ level. Those lines with it as the upper level, the $2.13/14 \mu\text{m}$ and $2.40/41 \mu\text{m}$ doublets (see Figs 1 and 2) are much stronger than those with it as the lower level (H band lines), revealing that pumping through the resonance $3s^2S-5p^2P$ line must be a significant populator of the $5p^2P$ levels. Pumping through the $3s^2S[1/2]-5p^2P[3/2]$ 1025.968\AA transition is very efficient due to $\text{Ly}\beta$ fluorescence. This was confirmed in models in which we decoupled the $5p^2P[3/2]$ and $5p^2P[1/2]$ levels (see Fig. 6), resulting in Mg II $2.13/14 \mu\text{m}$ ratios much higher than observed.

The relevance of this process can be easily followed in Fig. 6, which displays the behavior of the doublet as a function of the choice of the Mg II atom and the turbulent velocity. The latter refers to the fixed Doppler width used in our models to compute the level populations. In the left panel of Fig. 6 the levels are considered to be decoupled (i.e., the number of superlevels in the model atom, NS, is set to the total number of levels in the full atom, NF). Because $\text{Ly}\beta$ lies closer to $3s^2S[1/2]-5p^2P[3/2]$ ($\Delta v=72\text{km s}^{-1}$) than to $3s^2S[1/2]-5p^2P[1/2]$ ($\Delta v=114\text{km s}^{-1}$), and because in these LBVS the terminal velocities and wind densities determine the line formation zones), only the $5p^2P[3/2]$ is pumped thru fluorescence. Indeed, it can be seen that as the turbulence velocity is increased, the overlap between $\text{Ly}\beta$ and the Mg II line increases, as does the population of the $5p^2P[3/2]$ level and the strength of the Mg II $2.13 \mu\text{m}$ line increases, while the longer wavelength Mg II $2.14 \mu\text{m}$ line is unaffected. On the other hand, if the Mg II model atom has both levels combined into a superlevel (NS=NF, Fig. 6-right), the observed ratio is reproduced. Furthermore, increasing the turbulent velocity, and hence the effect of fluorescence, increases the pumping of both levels equally and thus

⁴We think that the slight mismatch in the Fe II] $2.117 \mu\text{m}$ line in both objects is related to the accuracy of the f value.

increases the strength of the doublet with a constant ratio between its components. From Fig. 6 it can be seen that our assumed collision coefficients connecting the Mg II $5p^2P[1/2]$ and $5p^2P[3/2]$ levels may be too low. This comparison illustrates the importance of making the correct choice of model atoms for quantitative spectroscopic analysis.

Due to fluorescence coupling, the Mg II K-band lines show a stronger dependence on turbulent velocity than do the H-Band lines. We estimate about twice solar Mg abundance and an associated uncertainty (see Fig. 7) of about ± 0.25 dex (due to uncertainties related to the fluorescence contribution).

Silicon. The Si II doublet $5s^2S_{1/2}-5p^2P_{3/2}$ $1.691 \mu\text{m}$ and $5s^2S_{1/2}-5p^2P_{1/2}$ $1.698 \mu\text{m}$ constitutes a powerful diagnostic tool, as it appears in emission for only a very narrow range of stellar temperatures and wind density structures, indicating the presence of amplified NLTE effects. However, since it forms at the base of the wind, its strong dependence on the details of the velocity field there hinders a precise silicon abundance determination.

Instead, we use the well-behaved recombination line Si II $3s^26g^2G-3s^25f^2F$ at $1.718 \mu\text{m}$ which shows a stronger dependence on the silicon abundance. Once again, a realistic mapping of full- to super-levels in our model atom is required. From our model fits (see Figs. 1 and 2) we derive roughly twice solar abundance (± 0.20 dex) for silicon in each LBV, similar to magnesium (see Fig. 7).

Other elements. One might expect a number of oxygen lines might be detectable in infrared spectra of LBVs: i.e., strong O I lines at $2.763 \mu\text{m}$, $2.893 \mu\text{m}$ and $3.098 \mu\text{m}$ and weaker lines at $1.8243 \mu\text{m}$, $3.661 \mu\text{m}$ and $3.946 \mu\text{m}$. Several of these, but not all, are problematical from ground-based observatories. Unfortunately our data set only encompasses the O I $1.745 \mu\text{m}$ line which is blended with a stronger Mg II line. Thus, we defer an attempt to estimate the oxygen abundance until high resolution observations of unblended lines can be obtained. Determining the oxygen abundances in these objects will provide crucial constraints on their evolutionary status. Models show that when $H/He < 1.50$ oxygen has reached its maximum depletion within CNO equilibrium, while a significantly higher O content should be present on the stellar surface for H/He values around 3. The results in Table 1 then predict that the Pistol Star and FMM362 have different oxygen abundances. On the other hand, if an LBV has a $H/He < 1.50$ but is still hydrogen rich, the oxygen abundance determination, expected to be ~ 0.04 of the original value, will provide a measure of the metallicity of the natal cloud. High resolution L-Band spectra of the Pistol Star should be able to address this issue.

The only detected sodium lines are the well-known doublet at $2.206/9 \mu\text{m}$, from which we obtain a very high abundance, $\sim 20 \times$ solar. The strong observed emission of this doublet

in the K-band spectra of other LBVs has been noted previously by Hillier et al. (1998). Interestingly, our models display only a minor dependence of these lines on clumping. On the other hand, the strengths of the sodium lines might not indicate extraordinary sodium abundance if the lines are produced by fluorescence of circumstellar material, a component that we do not model.

5. Discussion.

Our results suggest solar Fe abundances and approximately twice-solar α -element abundances for the Quintuplet LBVs. Presumably, these abundances were the same in the gas that condensed to form these stars and the other stars in the Quintuplet cluster and indeed in the whole of the present-day Galactic center. The results can be discussed in the context of similar measurements of Galactic center objects and with respect to the trend one might expect if the region is an inward extension of the disk or the bulge. In addition, the ratio of Fe to α -elements might be used to decipher the star formation history in the Galactic center.

Table 2 displays a number of recent determinations of stellar metal abundances in the Galactic Center together with the above mentioned three reference patterns for solar abundances. The values derived for Fe abundances in cool stars agree with our result (Carr et al. 2000; Ramirez et al. 1997, 1999, 2000). Cunha et al. (2007) find a very narrow range of Fe abundances clustered around the solar value for a population of cool stars in the central 30 pc. Of particular interest is star VR5-7 from Cunha et al. (2007) sample which is located in the Quintuplet Cluster and shows $A(\text{Fe}/\text{H})=7.60$ and $A(\text{Ca}/\text{H})=6.41$

There are relatively few measurements of the α -element abundances ($[\alpha/\text{Fe}]$) in GC stars. Najarro et al. (2004) find solar abundances (as defined in this paper) for hot stars in the Arches cluster based on the oxygen abundance and, to a lesser degree, carbon abundance, and adopting the canonical solar value of $A(\text{O}/\text{H})=8.93$ (Anders & Grevesse 1989). Those estimates assume that nitrogen has reached its maximum surface abundance value. Evolutionary models indicate that 95% of that value is already attained by the time that $\text{H}/\text{He}<2$ (by number). Najarro et al. (2004) followed the metallicity patterns from the Geneva evolutionary models and assumed no selective enrichment of CNO or α -elements vs Fe, in concluding that the stars in the Arches Cluster have solar α -element abundances. However, estimates of solar abundances have varied considerably over the past 15 years (e.g. Allende Prieto 2008, see also Table 2). Thus, depending on the assumed solar CNO composition, the derived nitrogen abundance by Najarro et al. (2004) could imply solar (Anders & Grevesse 1989), $1.2 \times$ solar (Grevesse & Noels 1993) or $2.0 \times$ solar (Asplund et al. 2005) CNO composition.

Table 2. Metallicity Estimates in the GC

	A(Fe/H)	A(O)	Σ CNO	Z(N)	A(Mg/H)	A(Si/H)	A(Ca/H)
Sun							
Anders & Grevesse (1989)	7.67	8.93	1.6	1.5	7.58	7.55	6.36
Grevesse & Noels (1993)	7.50	8.87	1.4	1.3	7.58	7.55	6.36
Asplund et al. (2005)	7.45	8.66	0.82		7.53	7.51	6.31
Hot Stars							
This work	7.54±0.15				7.85	7.84	
Najarro et al. (2004)				1.57±0.45			
Geballe et al. (2006)		8.91±0.12					
Martins et al. (2007a)				1.43±0.42			
Martins et al. (2007b)				1.80±0.50			
Cool Stars							
Carr et al. (2000)	7.48±0.13		1.14±0.55				
Ramirez et al. (2000)	7.61±0.22						
Cunha et al. (2007)	7.59±0.06	9.04±0.19					6.71±0.14

Note. — Compilation of estimated stellar metal abundances at the GC. All abundances are given as A(X/H) except column 4 which displays the total CNO mass percentage and column 5 displaying the nitrogen surface abundance percentage Z(N). For the first two rows (solar values), column 5 gives the maximum nitrogen surface mass abundance, $Z(N)_{max}$, reached during evolution according to the Geneva models. For the other rows, the average of the derived Z(N) for the sample in each work is displayed. All studies of hot stars make use of CMFGEN, while those of cool stars utilize Plez (1992) models grid. The results of Najarro et al. (2004) and Martins et al. (2007b) are for stars in the Arches Cluster while those of Geballe et al. (2006) and Martins et al. (2007a) refer to the Central Parsec Cluster. Star AFNW in Martins et al. (2007a) has not being considered due to the poorer S/N and resolution quoted by the authors. The results of Carr et al. (2000) are for IRS7 while those of Ramirez et al. (2000) are for six M supergiants and three giants. Cunha et al. (2007) extends the sample of Ramirez et al. (2000) and also computes CNO and α -elements abundances.

Recently Martins et al. (2007a,b) have analyzed a larger sample of hot stars in the Arches and Central Parsec clusters and find similar results (see Table 2). Interestingly, if one considers only the objects in Martins et al. (2007b) with $\text{He}/\text{H} > 0.1$ and those with $\text{Z}(\text{C}) < 0.05$, i.e., fulfilling the condition to be close enough to $\text{Z}(\text{N})_{\text{max}}$, the average value of $\text{Z}(\text{N})$ is 1.7.

Geballe et al. (2006) estimate roughly solar oxygen abundance, $\text{A}(\text{O}/\text{H})=8.91$, in IRS 8, an OIf supergiant near the central parsec. Cunha et al. (2007) find $\langle \text{A}(\text{O}/\text{H}) \rangle = 9.04$ ([0.37]) and $\langle \text{A}(\text{Fe}/\text{H}) \rangle = 7.59$ ([0.14]) for their sample of cool stars, where the numbers in brackets are the ratio with respect to the solar value in dex. This implies $[\text{O}/\text{Fe}] = 0.22$, i.e. a clear enhancement over the solar ratio. Again, the Cunha et al. (2007) measurements could be interpreted as indicating solar ratios in O over Fe if the solar O abundance in evolutionary models is used. It is crucial to have accurate solar abundances, and that values used in stellar evolution calculations should be consistent with these. An excellent example is attempting to determine whether the possible oxygen enhancement is due to a top-heavy IMF favoring α -elements vs Fe enrichment, or simply an overall CNO and metal enhancement. Thus, taking the CNO abundances for the GC objects from Cunha et al. (2007) and assuming C/N equilibrium values one can interpret their results either as solar CNO with mildly enhanced (30%) oxygen (Anders & Grevesse 1989) or a clearly supersolar environment with a factor of 1.7 enhancement for C and N and 2.5 for oxygen (Asplund et al. 2005).

Fortunately, there are other α -elements whose adopted solar abundances have suffered basically no major revision. Thus, we believe that the enhanced values obtained in this work for Mg and Si, roughly a factor of two solar, together with the enhancement of Ca found by Cunha et al. (2007), are a strong indication of the enrichment of α -elements compared to Fe.

Our results run counter to the trend in the disk (Rolleston et al. 2000; Smartt et al. 2001; Martín-Hernández et al. 2003), and are more consistent with the values found for the bulge (Frogel et al. 1999; Feltzing & Gilmore 2000). This may imply that the ISM in the disk does not extend inward to the GC, so that material is dragged into the central molecular zone from the bulge rather than from the disk. Another possibility is that the GC stars are forming out of an ISM that has an enrichment history distinctly different from that of the disk. At this point, further studies of the α -elements vs Fe would be useful. Future high S/N and high resolution spectroscopy of the O I lines in LBVs and K-band spectroscopy of WNL stars in the same cluster (Najarro et al. in prep.) will provide two independent measurements of the original oxygen content, and thus set definite constraints on metallicity.

The modest enrichment in α -elements versus Fe that we find in the two Quintuplet LBVs is consistent with a top-heavy IMF in the GC (Figer et al. 1999a). In such a scenario,

enhanced yields of α -elements compared to Fe are expected through a higher than average ratio of the number of SNII vs SNIa events (Wheeler et al. 1989; Cunha et al. 2007).

We thank Fabrice Martins and Katia Cunha for useful discussions. F. N. acknowledges AYA2004-08271-C02-02 and AYA2007-67456-C02-02 grants. The material in this paper is based on work supported by NASA under award NNG 05-GC37G, through the Long Term Space Astrophysics program. TRG's research is supported by the Gemini Observatory, which is operated by the Association of Universities for Research in Astronomy, Inc., on behalf of the international Gemini partnership of Argentina, Australia, Brazil, Canada, Chile, the United Kingdom, and the United States of America. D. Figer is supported by a NYSTAR Faculty Development Program grant.

REFERENCES

- Afflerbach, A., Churchwell, E. B. & Werner, M.W., 1997, *ApJ*, 478, 190
- Allende Prieto, C. 2008, 14th Cambridge Workshop on Cool Stars, Stellar Systems, and the Sun, 384, 39
- Anders, E. & Grevesse, N., 1989, *Geochimica et Cosmochimica Acta*, Vol. 53, 197
- Asplund, M., Grevesse, N., & Sauval, A. J. 2005, *Cosmic Abundances as Records of Stellar Evolution and Nucleosynthesis*, ASPC, 336, 25
- Carr, J.S., Sellgren, K. & Balachandran, S.C. 2000, *ApJ*, 530, 307
- Charbonnel, C., Meynet, G., Maeder, A., Schaller, G., & Schaerer, D. 1993, *A&AS*, 101, 415
- Cunha, K., Sellgren, K., Smith, V. V., Ramirez, S. V., Blum, R. D., & Terndrup, D. M. 2007, *ArXiv e-prints*, 707, arXiv:0707.2610
- Cotera, A. S., Erickson, E. F., Allen, D. A., Colgan, S. W. J., Simpson, J. P., & Burton, M. G. 1994, *NATO ASIC Proc. 445: The Nuclei of Normal Galaxies: Lessons from the Galactic Center*, 217
- Crowther, P. A., Lennon, D. J., & Walborn, N. R. 2006, *A&A*, 446, 279
- Feltzing, S., & Gilmore, G. 2000, *A&A*, 355, 949
- Figer, D. F., McLean, I. S., & Morris, M. 1995, *ApJ*, 447, L29
- Figer, D. F., Najarro, F., Morris, M., McLean, I. S., Geballe, T. R., Ghez, A. M., & Langer, N. 1998, *ApJ*, 506, 384

- Figer, D. F., McLean, I. S., & Najarro, F. 1997, *ApJ*, 486, 420
- Figer, D. F., Kim, S. S., Morris, M., Serabyn, E., Rich, R. M., & McLean, I. S. 1999a, *ApJ*, 525, 750
- Figer, D. F., McLean, I. S., & Morris, M. 1999, *ApJ*, 514, 202
- Figer, D. F., Morris, M., Geballe, T. R., Rich, R. M., Serabyn, E., McLean, I. S., Puetter, R. C., & Yahil, A. 1999b, *ApJ*, 525, 759
- Figer, D. F., et al. 2002, *ApJ*, 581, 258
- Frogel, J.A., Tiede, G.P., & Kuchinski, L.E. 1999, *AJ*, 117, 2296
- Fuhrmann, K., 1998, *A&A*, 338, 161
- Geballe, T. R., Najarro, F., & Figer, D. F. 2000, *ApJ*, 530, L97
- Geballe, T. R., Najarro, F., Rigaut, F., & Roy, J.-R. 2006, *ApJ*, 652, 370
- Girardi, L., Bressan, A., Bertelli, G., & Chiosi, C. 2000, *A&AS*, 141, 371
- Glass, I. S., Catchpole, R. M., & Whitelock, P. A. 1987, *MNRAS*, 227, 373
- Glass, I. S., Moneti, A., & Moorwood, A. F. M. 1990, *MNRAS*, 242, 55P
- Glass, I. S., Matsumoto, S., Carter, B. S., & Sekiguchi, K. 1999, *MNRAS*, 304, L10
- Grevesse, N., & Noels, A. 1993, *Origin and evolution of the elements: proceedings of a symposium in honour of H. Reeves, held in Paris, June 22-25, 1992*. Edited by N. Prantzos, E. Vangioni-Flam and M. Casse. Published by Cambridge University Press, Cambridge, England, 1993, p.14, 14
- Grevesse, N., & Sauval, A. J. 1998, *Space Science Reviews*, 85, 161
- Groh, J. H., Hillier, D. J., & Damineli, A. 2006, *ApJ*, 638, L33
- Herald, J. E., Hillier, D. J., & Schulte-Ladbeck, R. E. 2001, *ApJ*, 548, 932
- Hillier, D. J. & Miller, D. L. 1998, *ApJ*, 496, 407
- Hillier, D.J., Crowther, P.A., Najarro, F., Fullerton, A.W., 1998b, *A&A*, 340, 483
- Hillier, D. J. & Miller, D. L. 1999, *ApJ*, 519, 354
- Hillier, D. J., Davidson, K., Ishibashi, K., & Gull, T. 2001, *ApJ*, 553, 837

- Iglesias, C. A., & Rogers, F. J. 1996, *ApJ*, 464, 943
- Kennicutt, R.C., Bresolin, F., Garnett, D.R. 2003, *ApJ*, 591, 544
- Kudritzki, R.-P., & Puls, J. 2000, *ARA&A*, 38, 613
- Luck, R. E., Kovtyukh, V. V., & Andrievsky, S. M. 2006, *AJ*, 132, 902
- Maciel, W.J., & Quireza, C. 1999, *A&A*, 345, 629
- Maeda, Y., et. al., 2002, *ApJ*, 570, 671
- Martín-Hernández, N.L., van der Hulst, J.M., & Tielens, A.G.G.M., 2003, *A&A*, 407, 957
- Martins, F., Genzel, R., Hillier, D. J., Eisenhauer, F., Paumard, T., Gillessen, S., Ott, T., & Trippe, S. 2007, *A&A*, 468, 233
- Martins, F., Hillier, D. J., et al., 2007, *A&A*, (submitted)
- Meynet, G., Maeder, A., Schaller, G., Schaerer, D., & Charbonnel, C. 1994, *A&A Supp.*, 103, 97
- Meynet, G., & Maeder, A. 2003, *A&A*, 404, 975
- Meynet, G., & Maeder, A. 2005, *A&A*, 429, 581
- Moneti, A., Glass, I. S. & Moorwood, A. F. M. 1994, *MNRAS*, 268, 194
- Nagata, T., Woodward, C. E., Shure, M., Pipher, J. L., & Okuda, H. 1990, *ApJ*, 351, 83
- Najarro, F., Hillier, D. J., Figer, D. F., & Geballe, T. R. 1999, *The Central Parsecs of the Galaxy*, ASPC, 186, 340
- Najarro, F. 2001, *P Cygni 2000: 400 Years of Progress*, ASPC, 233, 133
- Najarro, F., Figer, D. F., Hillier, D. J., & Kudritzki, R. P. 2004 (Paper I), *ApJ*, 611, L105
- Nugis, T., Crowther, P. A., & Willis, A. J. 1998, *A&A*, 333, 956
- Okuda, H., et al. 1990, *ApJ*, 351, 89
- Pinsonneault, M. H., & Delahaye, F. 2006, *ArXiv Astrophysics e-prints*, arXiv:astro-ph/0606077
- Plez, B. 1992, *A&AS*, 94, 527

- Puls, J., Markova, N., Scuderi, S., Stanghellini, C., Taranova, O. G., Burnley, A. W., & Howarth, I. D. 2006, *A&A*, 454, 625
- Ramirez, S.V., Carr, J.S., Balachandran, S., Blum, R., & Terndrup, D.M. 1997, in *IAU Symp. 184, The Central Regions of the Galaxy and Galaxies*, ed. Y. Sofue (Dordrecht: Kluwer), 28
- Ramirez, S.V., Sellgren, K., Carr, J.S., Balachandran, S., Blum, R., & Terndrup, D.M. 1999, *ASP Conf. Ser. 186: The Central Parsecs of the Galaxy*
- Ramirez, S.V., Sellgren, K., Carr, J.S., Balachandran, S., Blum, R., Terndrup, D.M., & Steed, A., 2000, *ApJ*, 537,205
- Rolleston, W.R., Smartt, S.J., Dufton, P.L., & Ryans, R.S.I., 2000, *A&A*, 363, 537
- Runacres, M. C.,& Owocki, S. P. 2002, *A&A*, 381, 1015
- Rudolph, A. L., Fich, M., Bell, G. R., Norsen, T., Simpson, J. P., Haas, M. R., & Erickson, E. F. 2006, *ApJS*, 162, 346
- Salasnich, B., Girardi, L., Weiss, A., & Chiosi, C. 2000, *A&A*, 361, 1023
- Schaller, G., Schaerer, D., Meynet, G., & Maeder, A. 1992, *A&AS*, 96, 269
- Shields, J.C., & Ferland, G.J., 1994, *ApJ*, 430, 236
- Smartt, S.J., Venn, K.A., Dufton, P.L., Lennon, D.J., Rolleston, W.R., & Keenan, F.P., 2001, *A&A*, 367, 86
- Stahl, O., Jankovics, I., Kovács, J., Wolf, B., Schmutz, W., Kaufer, A., Rivinius, T., & Szeifert, T. 2001, *A&A*, 375, 54
- Urbaneja, M.A., Herrero, A., Bresolin, F., Kudritzki, R.P., Gieren, W., Puls, J., Przybilla, N., Najarro, F., Pietrzynski, G., 2005, *ApJ*, 622, 862
- Vink, J. S., & de Koter, A. 2002, *A&A*, 393, 543
- Wheeler, J. C., Sneden, C., & Truran, J. W., Jr. 1989, *ARA&A*, 27, 279

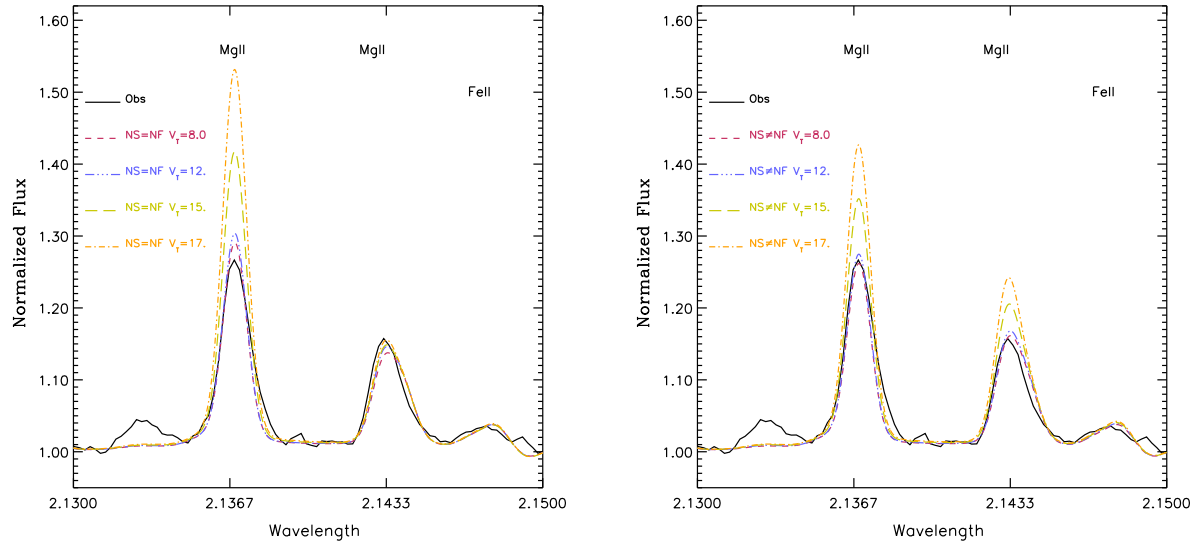


Fig. 6.— Influence of $\text{Ly}\beta$ fluorescence and choice of Mg II model atom on the Mg II K-band lines.

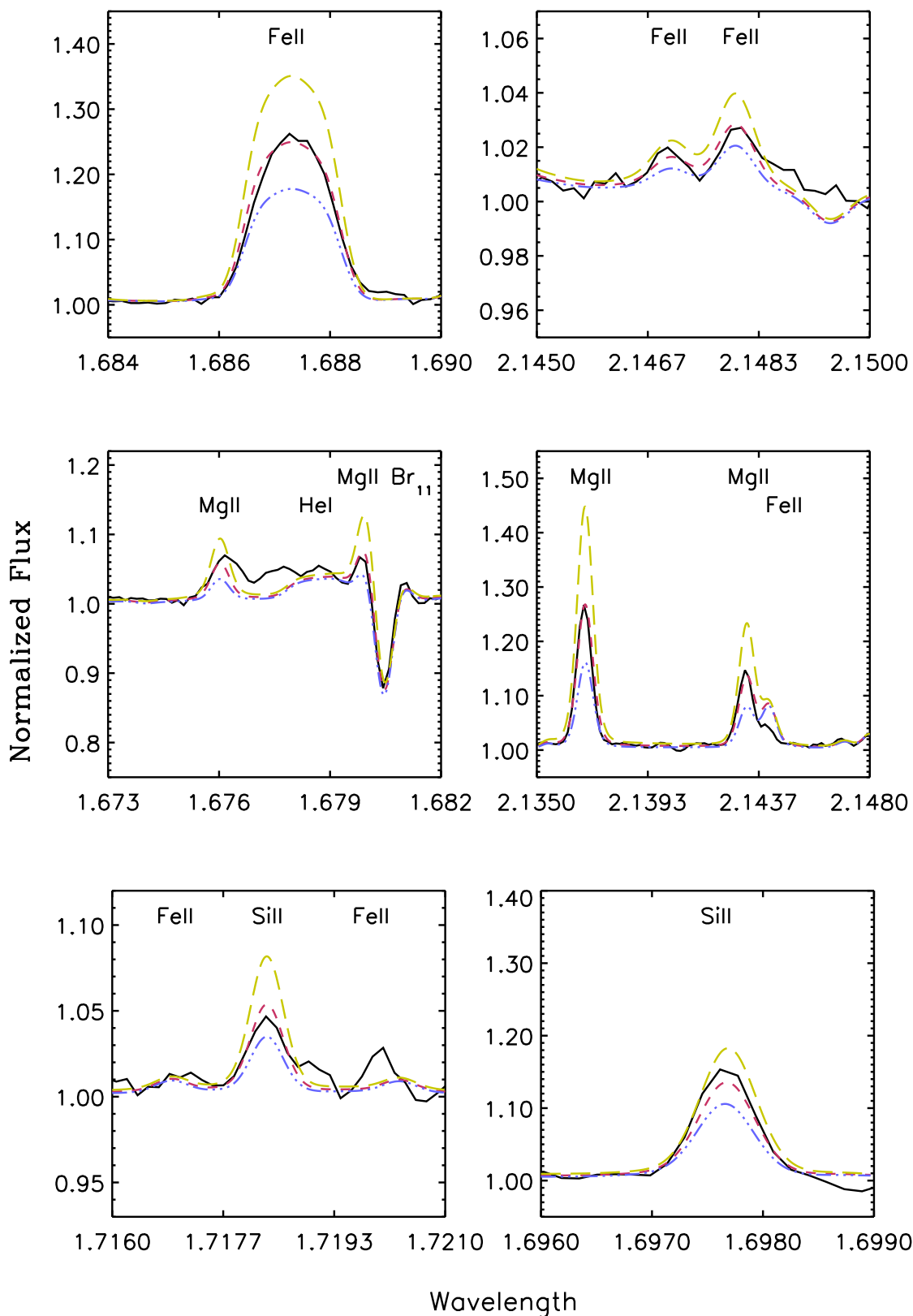


Fig. 7.— Error estimates of Fe (upper-panel), Mg (middle-panel) and Si (lower-panel) abundances. Dashed lines (red) correspond to our best model fitting the observed (black-solid) diagnostic lines of FMM362. Long-dashed (green) and dashed-dotted (blue) lines correspond to models where individual metal abundances have been set to the derived upper and lower